GEORG-AUGUST-UNIVERSITÄT
GÖTTINGEN

Bachelor's Thesis

Aktive Schwimmer in einem kugelförmigen Volumen

Active swimmers in a spherical volume

prepared at the Max Planck Institute for Dynamics
and Self-Organization by

Lea Luca Lenz

from Braunschweig

Submission date:	6th January 2016
Supervisor:	Dr. Marco G. Mazza
First Referee:	Dr. Marco G. Mazza
Second Referee:	Prof. Dr. Annette Zippelius

Contents

1 Introduction

The collective behaviour of active swimmers has received a lot of attention in the past years [1, 2]. Active swimmers are self-propelled particles, each having their own energy source which allows them to move individually, thus forming a nonequilibrium system. The collective dynamics of these particles are additionally influenced by many-body and hydrodynamic effects which complexify the system. Real-world examples for collective behaviour of active particles are bacteria [3], bird flocks [4] or migrating mammals [5] but also non-living systems like active nematic fluids [6] or traffic [7].

We study the behaviour of active swimmers confined to a spherical volume. The active swimmers in our case interact nematically which means they tend to align and move in parallel or anti-parallel directions. Similar systems have been investigated before with different boundary conditions. There have also been experiments and theoretical approaches and results concerning active swimmers confined to the surface of a sphere. We are among the first to look at a spherical volume as a constraint. The goal of this project is to find out how the behaviour changes for this curved and closed topology.

2 Theoretical background

We model the active swimmers as spherical, hardcore particles with a diameter $\sigma = 0.5$. The number of particles is varied and lies in the interval $[30^3, 51^3]$. They move within a spherical volume with a diameter $2R \geq 70\sigma$. The particles all have the same constant speed $v_0 = 0.5$ and each particle moves along its orientation vector $\hat{e_i}$. Chosing a constant speed is reasonable because at low Reynolds numbers fluctuations in the speed are exponentially damped and can thus be neglected. The direction of the velocity and the position are equally distributed in the initial state.

The particle-particle interaction is characterised by two potentials. The first is the Weeks-Chandler-Anderson (WCA) potential [8]

$$U_{WCA}(r) = \begin{cases} 4\varepsilon \left[\left(\frac{\sigma}{r}\right)^{12} - \left(\frac{\sigma}{r}\right)^{6} + \frac{1}{4} \right], & r < 2^{1/6} \\ 0, & r > 2^{1/6} \end{cases} \tag{1}$$

which describes the interaction between hardcore particles. When two particles collide, they are repelled. The WCA potential is equivalent to the repulsive part of the Lennard-Jones potential. The particles also have an orientational interaction described by the Lebwohl-Lasher potential

$$U = -\frac{1}{2} \sum_{i=1}^{N} \frac{1}{n_i} \sum_{j \in n_i} (\hat{e_i} \cdot \hat{e_j})^2 \tag{2}$$

which induces nematic alignment. The first sum runs over all N particles and the second one over the nearest neighbours n_i of particle i. We consider nearest neighbours all particles inside a sphere with radius $\epsilon = 1 = 2\sigma$ around the particle. Nematic alignment means that the particles tend to align and move parallelly or anti-parallelly. It is here used to describe the effects of the combined hydrodynamics on the particles.

As follows from the explanations above, the equations of motion for one particle i are given by

$$\dot{\boldsymbol{r}} = v_0 \hat{e_i}, \tag{3}$$

$$\dot{\hat{e_i}} = -\gamma \frac{\partial U}{\partial \hat{e_i}} + \boldsymbol{\xi_i}(t). \tag{4}$$

with $\hat{e_i}$ the unit vector of the orientation, U the Lebwohl-Lasher potential and $\boldsymbol{\xi_i}(t)$ the noise vector with random direction and absolute value η.

The interaction between the particles and the spherical wall is implemented through

elastic collisions. The particle's orientation is reflected at the tangent plane of the interaction point and the speed remains the same.

We perform molecular dynamics simulations with 200 000 time steps of length $\delta t = 0.1$. The equations of motion are integrated using an explicit Euler algorithm. To satisfy the constraints on the orientation vectors we use Lagrange-multipliers as in Ref. [9].

3 Recent research on active swimmers

3.1 Numerical investigation of point-like active nematic particles in a bulk

There has been considerable research in this area in the past years. A work very closely related to ours is the work of Breier *et al.* [10], where almost the same system to the one considered here was studied with the only differences that a different topology was used and the particles were considered point-like. They investigated particles in a bulk (periodic boundary conditions in all directions) and in a sandwich configuration (walls in the z-direction and periodic boundary conditions in the x- and y-direction). The results obtained in Ref. [10] is an important reference for putting our results into context.

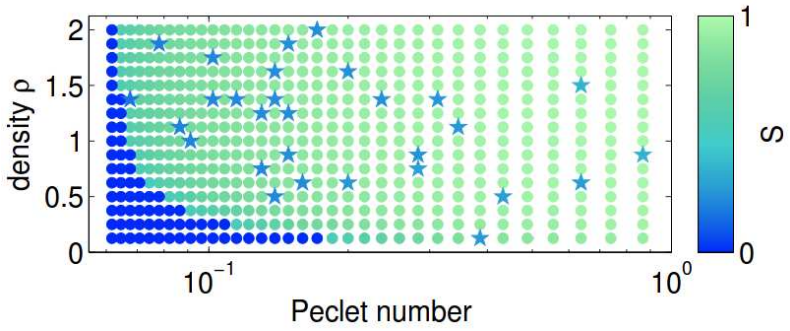

Figure 1: Phase diagram for pointlike particles in a bulk. The value of the global nematic parameter S is indicated by the colours. The stars mark chiral states. Source: Ref. [10].

A phase diagram was plotted by varying the number density $\rho \equiv \frac{N}{V}$ and the Péclet number

$$\mathcal{P} \equiv \frac{\text{advection}}{\text{diffusion}} = \frac{\epsilon v_0}{\epsilon^2 \eta^2 / \gamma} = \frac{v_0 \gamma}{\epsilon \eta^2}. \tag{5}$$

The variables have the same meaning as in our simulations (see Sec. 2). The density

ρ and the Péclet number $\mathcal{P}$ are two parameters commonly used to describe bacterial suspensions [11]. To quantify the state of the system they introduced the nematic order parameter S as the largest eigenvalue of the nematic order tensor

$$Q = \frac{1}{2N} \sum_{i=1}^{N} [3\hat{e}_i \otimes \hat{e}_i - \mathbb{I}], \tag{6}$$

where $\otimes$ denotes the tensor product, and $\mathbb{I}$ is the unit tensor. $S \in [0, 1]$ indicates how aligned the particles are with $S = 0$ indicating an isotropic state and $S = 1$ a perfectly aligned configuration. This order parameter is calculated for each pair $(\rho, \mathcal{P})$. The resulting phase diagram is shown in Fig. 1. As one can see there is a clear phase transition from an isotropic state to a nematic state. For very low Péclet numbers (which means high noise) the system is always in the isotropic state. When the Péclet number is large enough, the system is in the nematic state for all densities. This is consistent with the fact that a high Péclet number means low noise η and thus small fluctuations of the directors.

3.2 Experiments and simulations on motile bacteria in a droplet

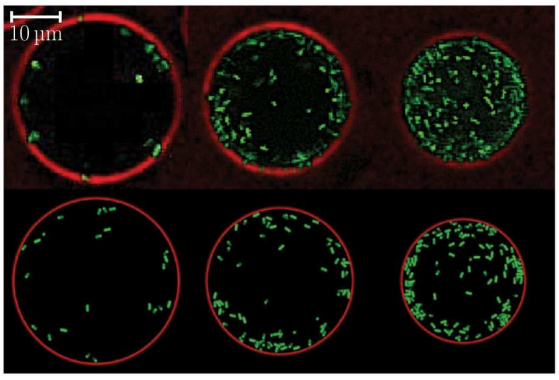

Figure 2

Recently, swimmers in a confined geometry have also been subject to investigation. In their experiments Vladescu *et al.* [12] studied *E. coli* bacteria confined within spherical droplets in a water-in-oil emulsion. The walls of the droplets were given by the interface of water and oil. They varied the average cell density ρ_0 and the radius R of the droplet. For small densities $\rho_0 \to 0$ they observed wall hugging, a peak of the density at the inner surface of the droplet. Increasing the average cell density, the density in the main part of the sphere increases uniformly. The density peak

at the inner surface survives and its absolute height increases whereas the relative peak $\frac{\rho}{\rho_0}$ decreases. They found this behaviour for all radii they studied. In the top of Fig. 2 one can see snapshots of the experiments.

Vladescu *et al.* were also able to reproduce their results in simulations. In their model the *E. coli* cells are trapped at the surface with a certain probability when arriving at an empty section of the surface. Once trapped at the surface, they move along the surface until they move away spontaneously or are scattered by another cell. Results of the simulations are shown in the bottom of Fig. 2.

3.3 Experiments with active nematic vesicles

Recently, swimmers in a confined geometry have also been subject to investigation. In experiments by Keber *et al.* [13] microtubules were attached to the inner surface of lipid vesicles, creating a dense monolayer of microtubules. Kinesin proteins supplied with energy by adenosine triphosphate (ATP) hydrolysis then wandered along these microtubules. The evolving structures were visualised with the help of confocal microscopy. From topology we know that it is impossible to spread parallel lines on a curved surface without a defect. For a sphere the sum of the charge of all the defects has to be $s = 2$ where $2\pi s$ describes the rotation angle of the director field. Basic nematic defects have a charge of $s = \pm\frac{1}{2}$ corresponding to a rotation of π. These defects will be placed in a way that minimises the free energy of the system. Under the assumption that the bend and splay elastic moduli are equal the most favourable defect configuration in equilibrium is given by four $+\frac{1}{2}$ defects placed at the corners of a tetrahedron. The tetrahedral structure appears because the defects repell each other and thus maximise their distances. These theoretical results were confirmed in experiments by Keber *et al.* [13].

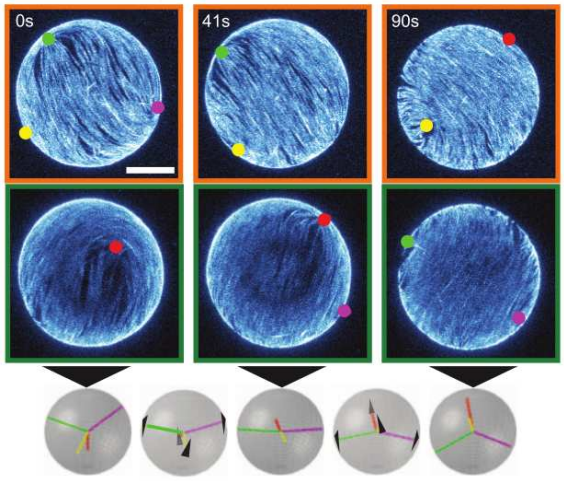

Figure 3: Hemispherical projections of a nematic vesicle. This shows a time series of projections over one oscillation period. The coloured dots mark the defects. One can see the system transforming from a tetrahedral to a planar and back to a tetrahedral structure. Source: Ref. [13].

They also observed the system for nonequilibrium conditions with finite ATP concentration. The resulting nematic stresses lead to motility of the four defects. For the same reason as in the equilibrium state the defects favour again a tetrahedral structure but with activity as an additional factor the defects start to move. As seen in Fig. 3 the defects move from a tetrahedral configuration to a planar configuration and then again to a tetrahedral one. This behaviour persists on large time scales. The system oscillates between these two states with a frequency depending on system size and ATP concentration.

They found that the radius of the vesicle influences the dynamics. For small radii they observed a band rotating around the equator.

3.4 Numerical approach on active swarms on a sphere

A more theoretical approach is given by the work of Sknepnek *et al.* [14]. They simulated self-propelled particles with polar alignment confined to the surface of a sphere. They studied the influence of the velocity v_0 of the particles, the noise and the size of the system.

For low velocity v_0 the particles form a polar vortex structure with two +1 defects at the poles. The particles move around the axis going through these poles. The particle velocity is decreasing from v_0 at the equator to zero at the poles. As v_0 is increased, the particles are compressed at the equator, forming a moving band with empty areas at the poles. Increasing v_0 further, the empty areas get bigger

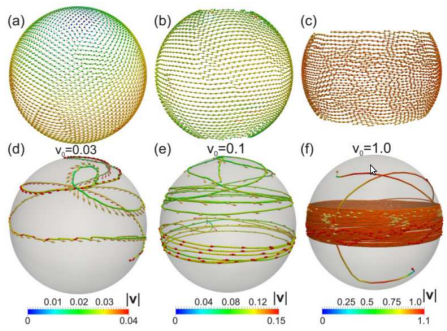

Figure 4: (a), (b) and (c) show the system for increasing v_0. (d), (e) and (f) show the trajectory of a single particle for the corresponding velocity. Source: Ref. [14].

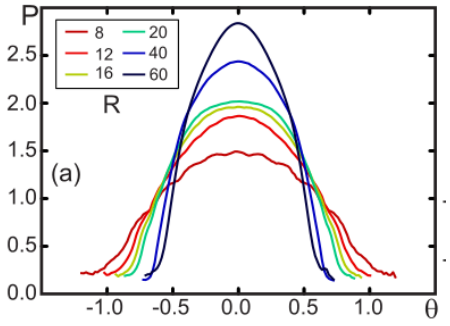

Figure 5: Pressure curves of the band for different radii. Source: Ref. [14].

and particles get more and more compressed as seen in Fig. 4. They compared their results to a planar counterpart of their system and could not find any similar phenomena appearing in flat space. In this way they could exclude other factors as a cause of the observed results and confirm that the formation of the polar vortex and the moving band is curvature-driven.

The system size influences the features of the band. For increasing radius R the width of the band decreases and the edge angles increase as seen in Fig. 5 and 6(a) and (b). As one would imagine, the band disappears for increasing noise as seen in Fig. 6(c)-(f).

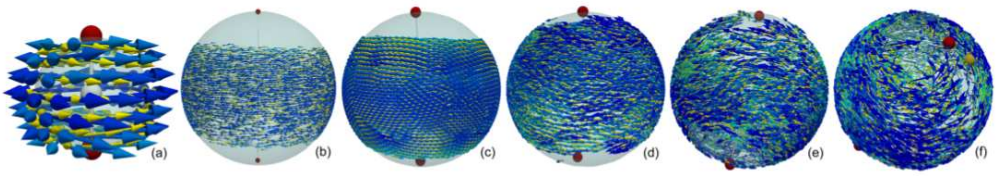

Figure 6: The influence of radius and noise. (a) and (b) are at a low noise strength at different radii. (c), (d), (e) and (f) are for the same radius but with increasing noise. Source: Ref.[14].

4 Method of investigation

We have now seen different ways of investigating active systems. As a first step, we want to find out if we can observe a phase transition as seen by Breier *et al.* [10]. We therefore set out to calculate a similar nonequilibrium phase diagram. The particles

in our system are of finite volume so instead of the density we use the filling fraction

$$\Phi = \frac{Nv}{V} \tag{7}$$

with v the volume of a single particle and $V = \frac{4}{3}\pi R^3$ the volume of the sphere. To gain a better understanding of the factors that lead to our results we vary the filling fraction in two different ways: By varying the radius of the sphere (see Sec. 5.1) and by varying the number of particles (Sec. 5.3). As an observable we use the nematic order parameter S (see Sec. 3.1). The order parameter is calculated every 500 time steps. To minimise the error due to fluctuations we calculate the time average over 50 000 time steps in the steady state of the system (see Sec. 5.1). Varying filling fraction Φ and Péclet number $\mathcal{P}$ (Eq. 5) and calculating the time average of the nematic order parameter S for each pair $(\mathcal{P}, \Phi)$ we then plot two phase diagrams. This gives us an overview of the particles' behaviour under different conditions. Further a phase diagram allows the comparison to results of Ref. [10].

We also take a closer look at the structures formed by the active particles as the nematic order parameter does not provide a unique characterisation of the system's state. It only indicates how aligned the particles are but not what topology they form. Therefore we take snapshots of the system for different parameters and times. To confirm the results we find in these snapshots and to investigate the time evolution of the system we create videos consisting of snapshots taken every 500 time steps.

5 Results

5.1 Varying Péclet number $\mathcal{P}$ and radius R

To make sure that we study the system in its steady state we plot the nematic order parameter S as a function of the time step (Fig. 7). We can see that the system has reached a steady state after 150 000 time steps for most values of $\mathcal{P}$ and Φ.

In Fig. 8 one can see the phase diagram in terms of Péclet number $\mathcal{P}$ and filling fraction $\Phi(R)$. We varied the filling fraction by varying the radius R of the sphere, the particle number is constant ($N = 27\,000$). The colour indicates the value of S. S is calculated every 500 time steps. For the phase diagram we average over 50 000 time steps in the steady state.

It is visible at first sight that large areas of the phase diagram are dark blue, corresponding to an order parameter $S \approx 0$ which describes an isotropic state. For filling fractions larger than $\Phi = 0.080$ the system is in an isotropic state for all values

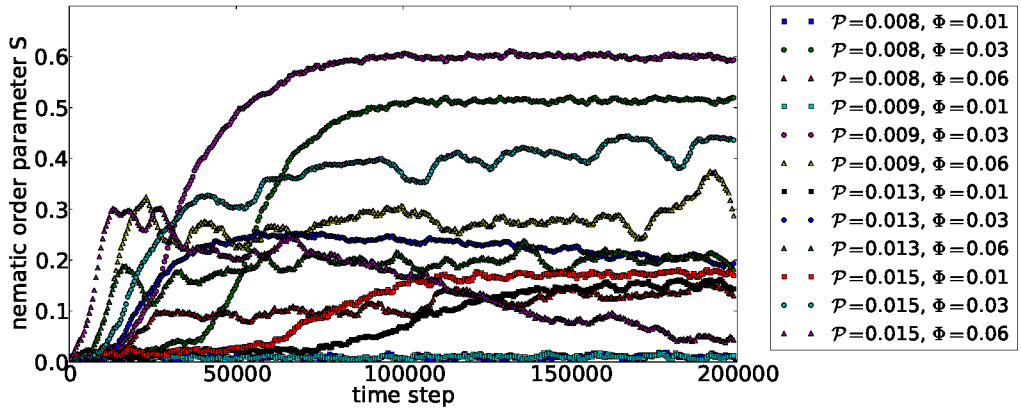

Figure 7: Temporal dependence of the nematic order parameter S for simulations at different $\mathcal{P}$ and Φ.

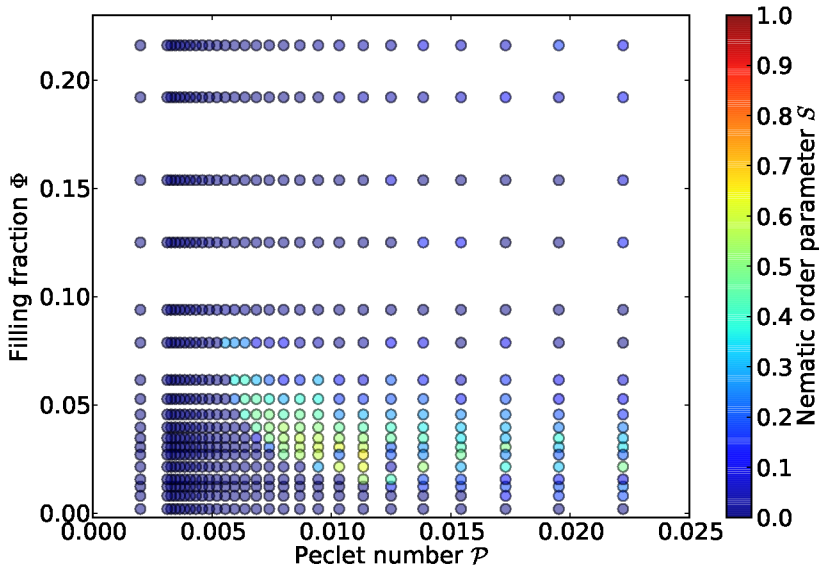

Figure 8: Phase diagram, plotted by varying Péclet number $\mathcal{P}$ and filling fraction $\Phi(R)$. The order parameter is indicated by the colourbar.

of $\mathcal{P}$. There is no phase transition. When the filling fraction is high, the particles collide often and their dynamics are frequently disturbed by these collisions. Because of this the formation of a pattern or structure is less likely or even impossible.

The active swimmers show a different behaviour for $\Phi \leq 0.08$. In Fig. 9 we see a close-up of this part of the phase diagram. We find an isotropic region for small values of $\mathcal{P}$ and Φ. For Péclet numbers $\mathcal{P} \leq 0.005 \Leftrightarrow$ noise $\eta \geq 3.1$ the system is always in the isotropic state, independent of the filling fraction. The reason for this is that the noise is so high that its influence is stronger than the influence of the nematic alignment. For $\Phi = 0.002$, the lowest filling fraction we investigated, the

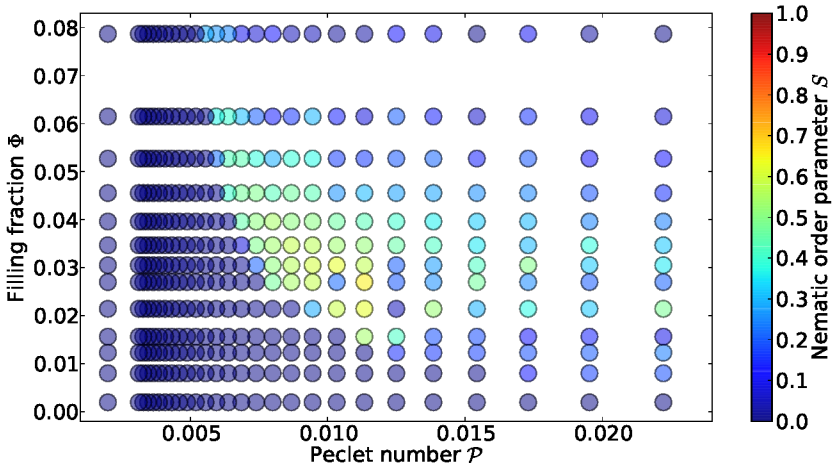

Figure 9: Close-up of the phase diagram in Fig. 8 showing the part of the diagram with a phase separation.

results are independent from the Péclet number as the system always stays in the isotropic state. This can be explained by the fact that the filling fraction is so low that the particles do not interact often enough to actually form a structure. For all filling fractions $0.002 \leq \Phi < 0.080$ we can see a clear transition from the isotropic state to a more ordered nematic state at a locus $\mathcal{P}_T(\Phi)$. We can see a bright region in the centre of the phase diagram, corresponding to an order parameter $0.5 \leq S \leq 0.65$. The highest values of S can be found for $\mathcal{P} \approx 0.11$ and $\Phi \approx 0.03$. In this region the system is in the nematic state for the largest interval of $\mathcal{P}$. For lower and higher filling fractions the Péclet interval corresponding to high order is smaller. For low filling fractions the boundaries of the highly ordered state become less clear.

Overall we see that with increasing values of $(\mathcal{P}, \Phi)$ there is a clear transition from an isotropic state to a nematic state and then a continuous transition back to a state with lower order parameter S.

In Fig. 10 we plot the nematic order parameter as a function of the Péclet number for some filling fractions. As we also saw in the phase diagram, the behaviour of the function differs depending on the filling fraction. All curves show a flat interval for low Péclet numbers and at some point a sharp increase of S. The higher the filling fraction, the lower the Péclet number at which this peak occurs. For a high filling fraction $\Phi = 0.079$ the peak is small and narrow. For lower filling fractions the peak first broadens and reaches higher values of S. Decreasing the filling fraction further, the course changes again. For $\Phi = 0.021$ there are several narrow peaks. For $\Phi = 0.016$ the peak still reaches a high value of S but then decreases rapidly.

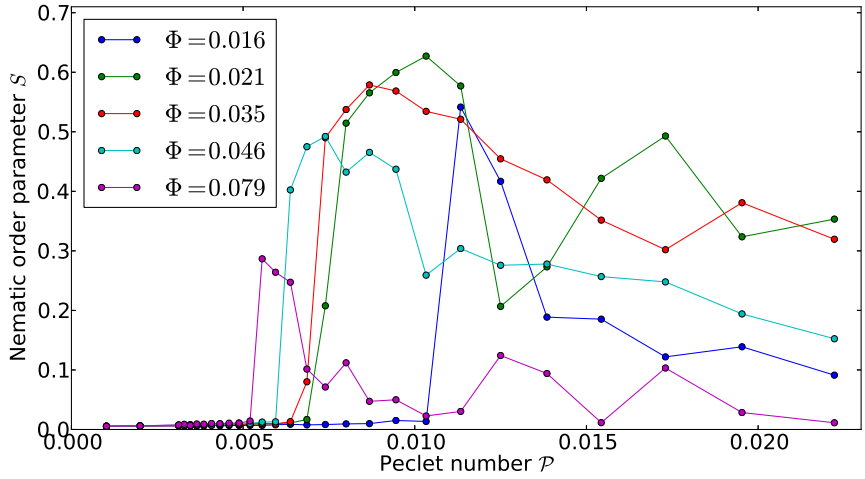

Figure 10: Dependence of the nematic order parameter S on the Péclet number $\mathcal{P}$ for various filling fractions.

All in all this figure confirms what we saw in the phase diagram.

5.2 Configurations

The phase diagram (Fig. 9) gives us a good overview of the states of the system. We find two phases, an isotropic and an ordered phase, and also a region of low order for high values of $(\mathcal{P}, \Phi)$. What we cannot see is what the value of the order parameter means for our system. We want to know what kind of configurations correspond to a certain S. To find out we take snapshots of the system in the steady state and create videos to examine the time evolution. A description of the videos can be found in the appendix of this thesis (Sec. A).

5.2.1 Structures in the steady state

The following observations were made after the transient, so after 100 000 time steps. At first we look at the isotropic state. In Fig. 11 we see a plot of the system with $\mathcal{P} = 0.005$ and $\Phi = 0.027$ after 150 000 integration steps. The blue arrows represent the orientation vectors $\hat{e}_i$ of the particles. The configuration looks as expected: Both particle positions and orientation vectors are equally distributed and we do not find any structure in this configuration.

Let us now take a look at the other states of the system. We can find four main structures in the ordered region of the phase diagram:

I A stream of particles going diametrically through the centre of the sphere, Fig. 12 and Video 1.

II A stream that splits up at one end, resulting in a Y-like structure, Fig. 13 and Video 2.

III A stream splitting up at both ends in orthogonal directions resulting in a tetrahedral structure, Fig. 14 and Video 3.

IV A band of particles moving at the surface of the sphere like a belt, Fig. 15 and Video 4.

The Y-like and the tetrahedral structure often show clusters in the centre. The geometries I, II and III also appear combined with the belt structure. Videos 5, 6 and 7 show these configurations.

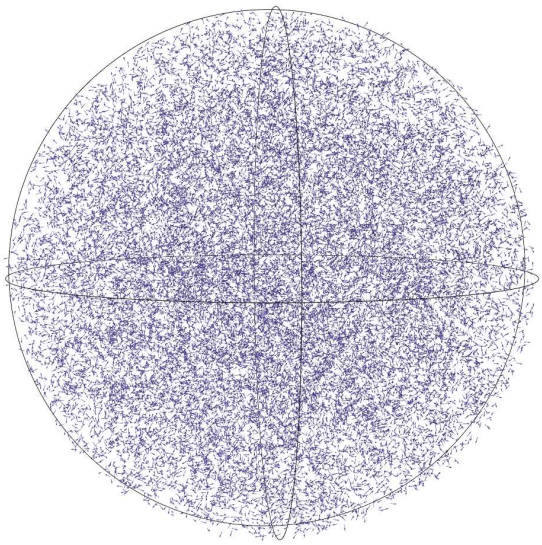

Figure 11: Snapshot of the system in the isotropic state with $\mathcal{P} = 0.004 \Leftrightarrow \eta = 3.4$ and $\Phi = 0.027$ after 150 000 time steps.

The occurrence of the structures and their combinations depend on filling fraction and Péclet number.

We start with our analysis at the upper left corner of the phase diagram, so for low Péclet number and high filling fraction. We already know what the isotropic state looks like so we start investigating at the phase transition line. At the low-$\mathcal{P}$ boundary of the nematic phase we find structures similar to Fig. 12. The stream is noisy close to the transition line and becomes more clear for larger values of $\mathcal{P}$. Increasing the Péclet number further we find the Y-structure and the tetrahedral structure. When we reach the region of the phase diagram where S decreases again an additional belt appears. The belt moves around the long axis of the Y or the tetrahedron, leading to structures as seen in Fig. 17 and 18.

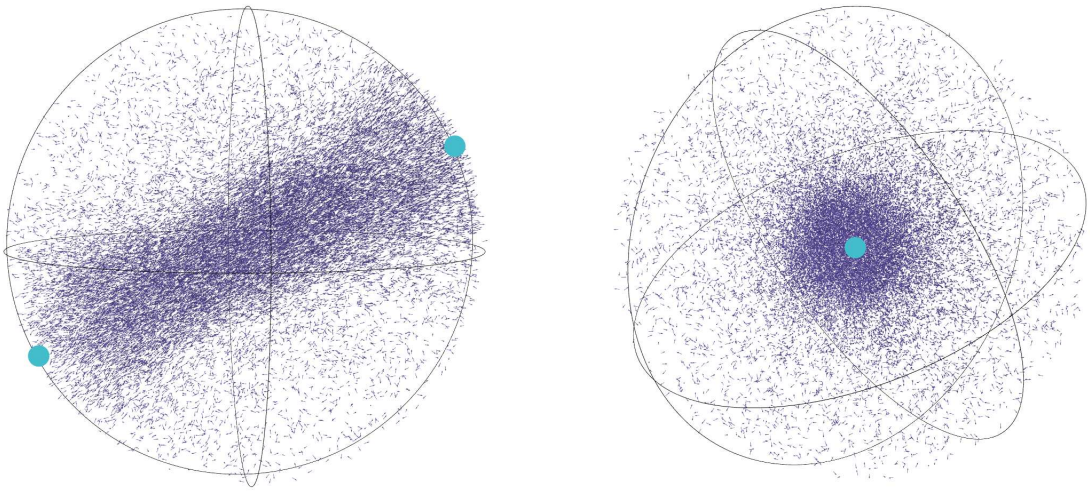

Figure 12: Snapshots of the system showing the stream configuration with $\mathcal{P} = 0.011$ and $\Phi = 0.021$ after 150 000 time steps from one side and rotated by 90°S. The coloured dots indicate the topological defects.

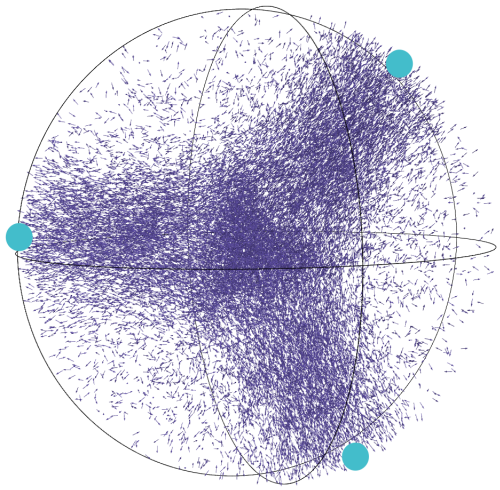

Figure 13: Snapshot of the Y-configuration after 150 000 time steps with $\mathcal{P} = 0.008$ and $\Phi = 0.062$.

This explains the lower order parameter for high values of $(\mathcal{P}, \Phi)$. The additional belt consists of particles moving in different directions than the particles in the main structure (e.g. stream). At this point it becomes clear why the nematic order parameter does not give a unique description of the system state.

For high filling fractions we often find clusters in the centre of the sphere. With decreasing filling fraction the clusters disappear which is plausible as a high filling fraction favours the formation of clusters. The tetrahedral structure appears less often and the stream becomes more important. The right edge of the ordered region is now dominated by configurations featuring a stream and a belt moving around

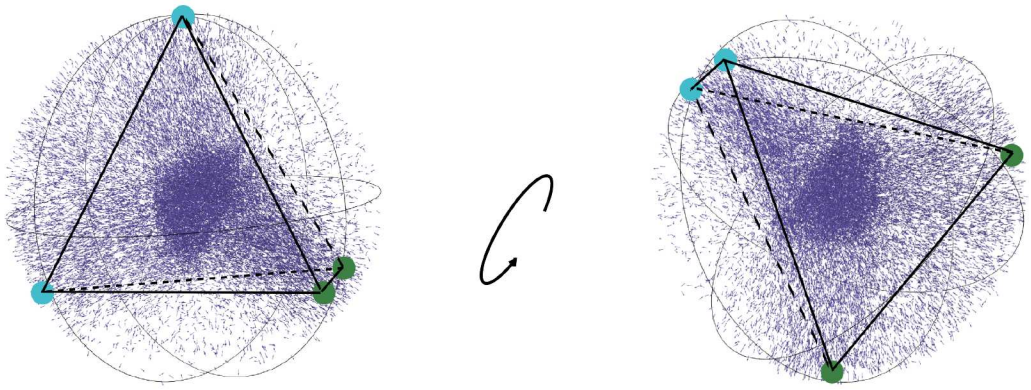

Figure 14: Snapshots of the system showing the tetrahedral structure with $\mathcal{P} = 0.010$ and $\Phi = 0.046$ after 150 000 time steps. The second picture shows the same configuration rotated by 90°. The blue dots define a plane P with the centre of the sphere, the green dots and the centre of the sphere lie in the plane $P_\perp$ orthogonal to P.

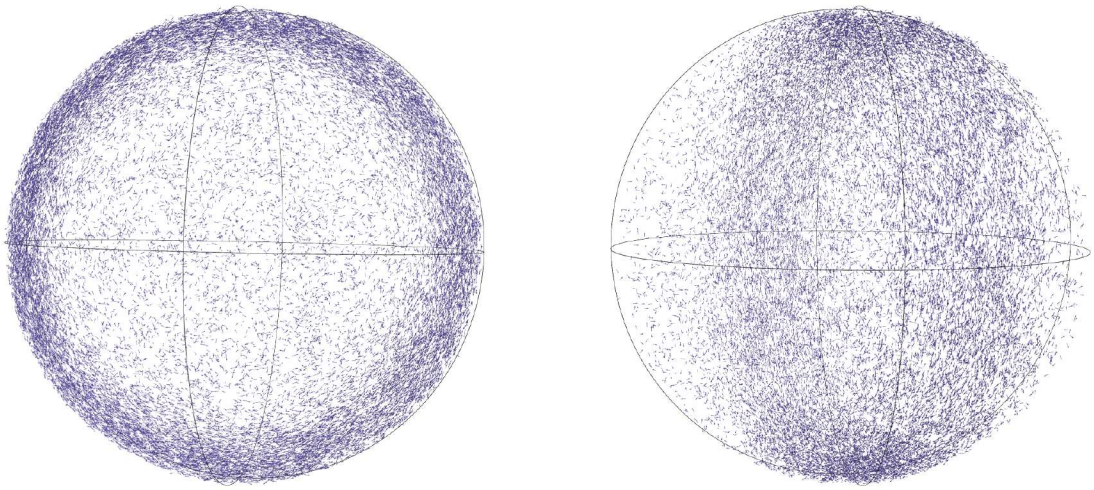

Figure 15: Snapshots of the system showing the belt configuration with $\mathcal{P} = 0.014$ and $\Phi = 0.016$ after 150 000 time steps from two different angles.

the stream axis as seen in Fig. 16. The configuration now transitions from a stream structure in the main part of the ordered state into a configuration with stream and belt for high Péclet numbers. For filling fractions smaller than $\Phi = 0.040$ the tetrahedron and the Y-structure do not appear at all. For filling fractions $\Phi \leq 0.016$ the belt also appears as a single phenomenon.

We have seen that the different structures occur for different parameters. The Y- and tetrahedral structure appear for high filling fractions and rather high Péclet numbers. The stream structure occurs for all filling fractions in the high noise regime, for low filling fractions also for low noise. The belt occurs for all filling fractions for high Péclet numbers. We mostly see it in combination with either

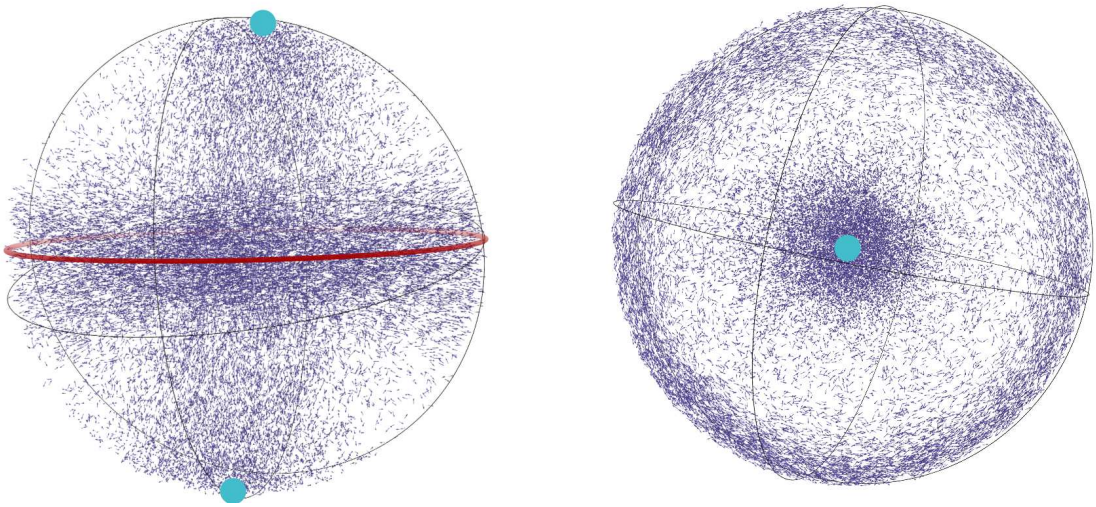

Figure 16: Snapshots of the system showing the stream and belt configuration combined with $\mathcal{P} = 0.013$ and $\Phi = 0.031$ after 150 000 time steps. The second picture shows the system after a rotation by 90°.

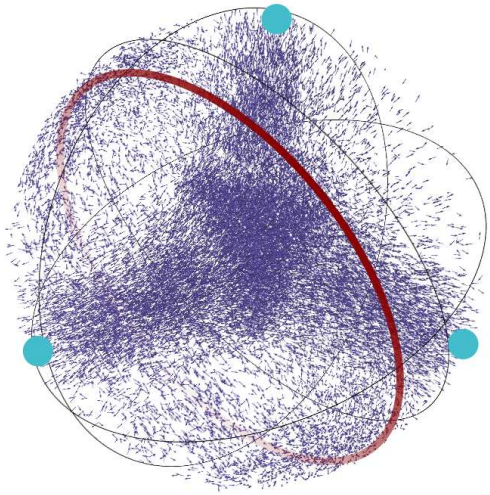

Figure 17: Snapshot of the Y-configuration and the belt combined after 150 000 time steps with $\mathcal{P} = 0.017$ and $\Phi = 0.062$.

stream, Y- or tetrahedral configuration, explaining the drop of the order parameter on the right handside of the phase diagram.

5.2.2 Evolution of the structures

The snapshots were all taken after 150 000 time steps in the steady state of the system. To learn more about the time evolution of the structures and the formation during the transient we created videos of the configurations.

We observe that the length of the transient depends on the parameters. The lower the Péclet number, the later the formation of the structure starts. For parameters

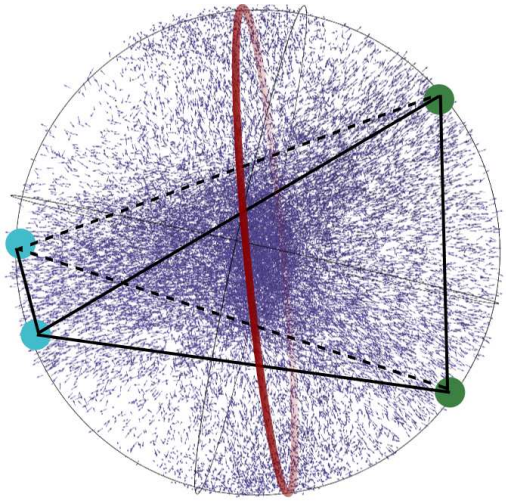

Figure 18: Snapshot of the tetrahedral configuration and the belt combined after 150 000 time steps with $\mathcal{P} = 0.017$ and $\Phi = 0.046$. Here again the blue dots define a plane P with the centre of the sphere, the green dots and the centre of the sphere lie in the plane $P_\perp$ orthogonal to P.

close to the phase transition line the structure becomes visible after 80 000 to 90 000 time steps whereas it only takes 25 000 steps for systems with the highest values of $\mathcal{P}$. This can also be seen in the Videos 8 and 9. An explanation for the different lengths of the transient could be the high noise at low Péclet numbers making it harder for structures to form and thus slowing down the process.

In systems with a high filling fraction the formation of clusters during the transient can be observed (see Video 10). For very high filling fractions clusters appear for all Péclet numbers in the nematic phase. They form during the transient and persist for the full length of our simulations. The clusters are always situated in the centre of the sphere, often at the branching point of a Y- or tetrahedral configuration (Fig. 13 and 14). In most cases there is only one cluster which is often disc-shaped. Sometimes we find two discs, arranged parallely as can be seen in Fig. 19. This structure does not persist, the two discs eventually merge into one cluster. For lower filling fractions ($\Phi \leq 0.031$) clusters only appear during the transient and vanish afterwards. There are only single clusters, often in the centre of a stream configuration.

The videos also let us observe the time evolution of the structures in the steady state. We find that the structures described in Sec. 5.2.1 persist for the full length of our simulations. Once the structure is formed there are only minor changes. As mentioned before, we observe that for systems close to the phase separation line the transient phase is longer and the formation of structures begins later. Due to this some of these systems have barely reached the steady state by the end of our

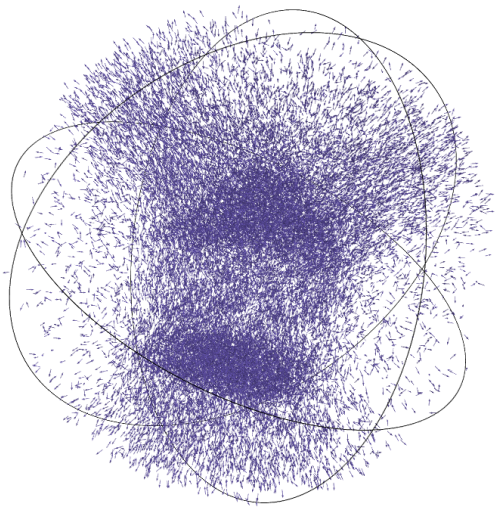

Figure 19: Snapshot of the system after 170 000 time steps with $\mathcal{P} = 0.009$ and $\Phi = 0.062$ showing two disc-like parallel clusters.

simulations. For example in Fig. 20 one can see the nematic order parameter as a function of time steps for a system with $\mathcal{P} = 0.007$ and $\Phi = 0.031$. As we averaged over the last 50 000 time steps for our phase diagram and the transient phase takes place in this interval, the calculated order parameter in Fig. 9 is misleading. To correct this, it would be necessary to run longer simulations for systems near the phase transition.

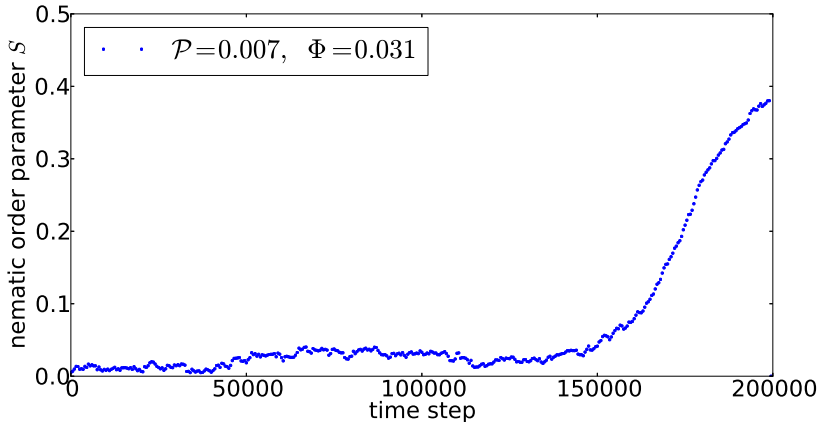

Figure 20: Temporal dependence of the nematic order parameter S for $\mathcal{P} = 0.007$ and $\Phi = 0.031$.

5.3 Varying Péclet number $\mathcal{P}$ and particle number N

In the previous sections we presented the results we obtained from varying the system parameters by changing the noise η (and thus the Péclet number $\mathcal{P}$) and

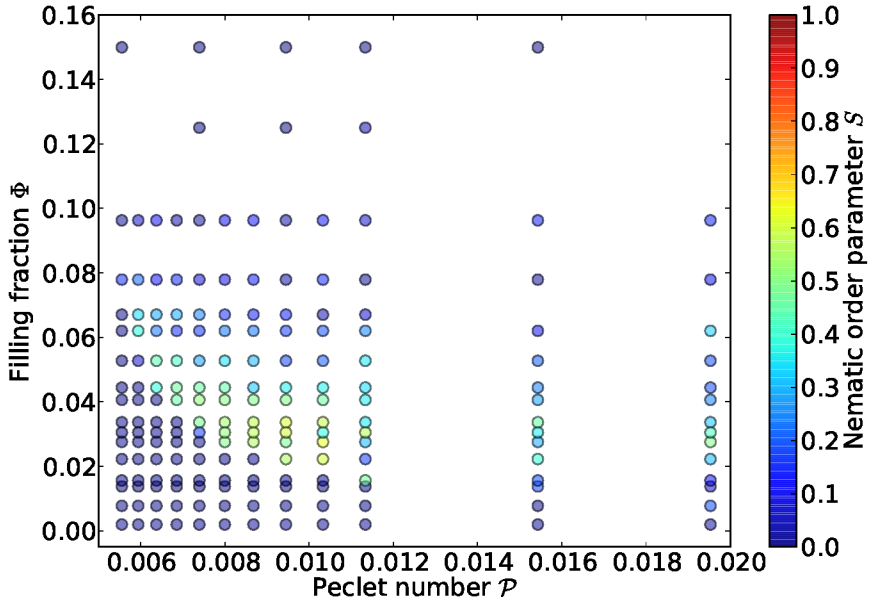

Figure 21: Phase diagram plotted by varying Péclet number P and the filling fraction as a function of the number of particles N. The colour indicates the nematic order parameter S.

the radius R (and thus the filling fraction Φ). By varying the radius we vary the curvature of the sphere

$$\kappa = \frac{2\sigma}{R}. \tag{8}$$

We want to find out in which way the observations we made in Sec. 5.1 were influenced by this change of curvature to find out as precisely as possible which factors lead to the formation of the structures. Therefore we plot another phase diagram, this time varying the filling fraction by varying the number of particles N instead of the radius. Of course the number of particles also influences the dynamics of the system but in combination with the previous results we have more information about the origin of the dynamic transitions.

The phase diagram in Fig. 21 and the one we study in Sec. 5.1 (Fig. 8) show similar features. There is an isotropic region for high filling fractions ($\Phi > 0.080$) where we do not see a phase transition. For lower filling fractions we find an isotropic region for small values of $(\mathcal{P}, \Phi)$. We also see a phase transition from this isotropic state to an ordered, nematic state and back to a less ordered state. One can find a close-up of this part of the phase diagram in Fig. 22. Comparing this close-up to the same section of the $(\mathcal{P}, \Phi(R))$ diagram, shown in Fig. 23, we notice that both diagrams look very similar. There are minor quantitative differences but both

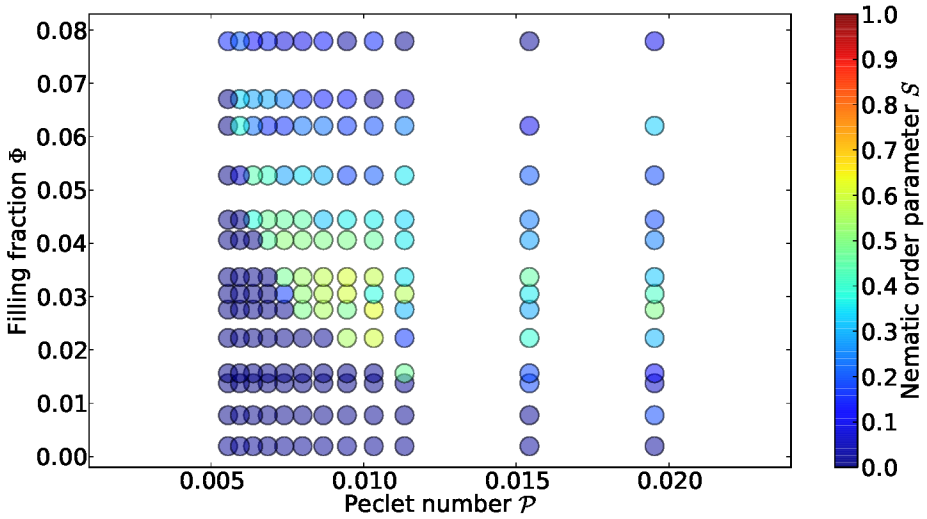

Figure 22: Close-up of the phase diagram plotted by varying Péclet number P and the filling fraction as a function of the number of particles N. The colour indicates the nematic order parameter S.

diagrams represent the same phenomenon. This leads to the assumption that the state of the system only depends on the Péclet number and the filling fraction and does in general not depend on the degree of curvature or the total particle number.

For a more quantitative comparison of the order parameter values of both diagrams we plot the order parameter as a function of the filling fractions $S(\Phi(N))$ and

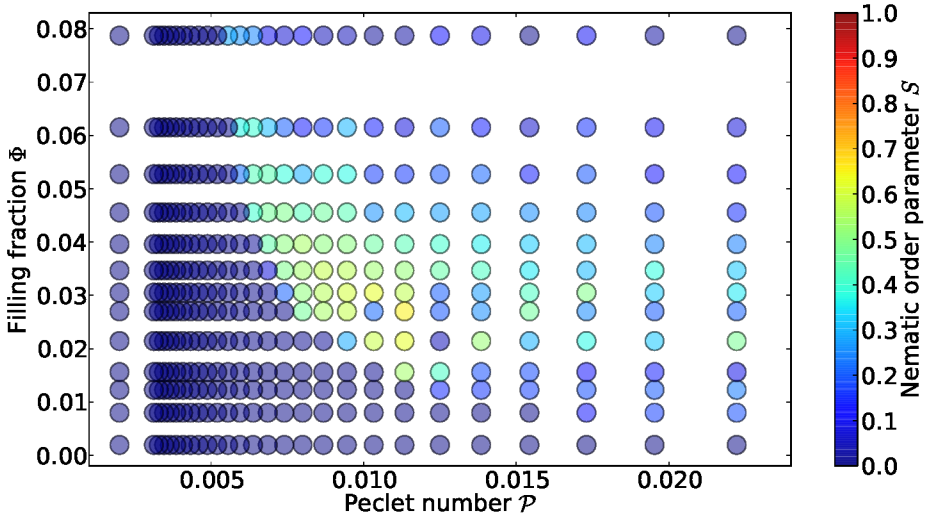

Figure 23: Close-up of the phase diagram plotted by varying Péclet number P and the filling fraction as a function of the radius R as seen in Sec. 5.1. The colour indicates the nematic order parameter S.

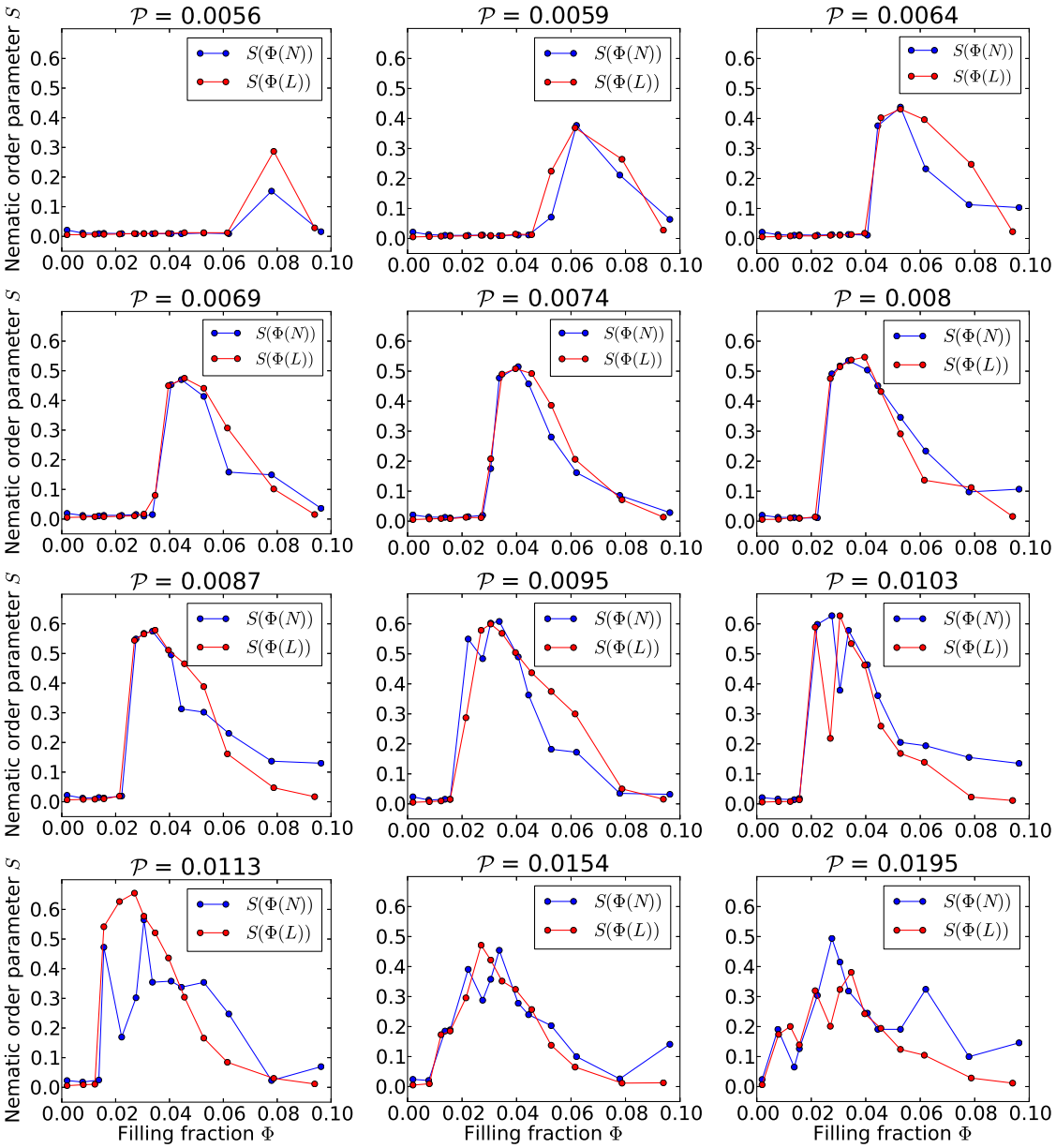

Figure 24: Comparison of the order parameters as a function of the filling fractions $S(\Phi(N))$ and $S(\Phi(R))$ for different Péclet numbers.

$S(\Phi(R))$ for the case when we vary N or R, respectively. In Fig. 24 one can see this comparison for different Péclet numbers. We notice that at low Péclet numbers the two graphs coincide for small filling fractions. For larger filling fractions they show a similar behaviour but also quantitative differences. With increasing Péclet number the graphs differ more and more. A possible explanation is that for high Péclet numbers and thus low noise the influence of the noise is so weak that other influences such as curvature and particle number determine the behaviour of the particles. Also at high Péclet numbers the graphs resemble most for small filling

fractions. An explanation for this could be that the denser the particles are packed, the more they interact with the walls. The geometry thus plays a more important role in systems with a high filling fraction.

5.4 Comparison of configurations with different curvature κ and particle number N

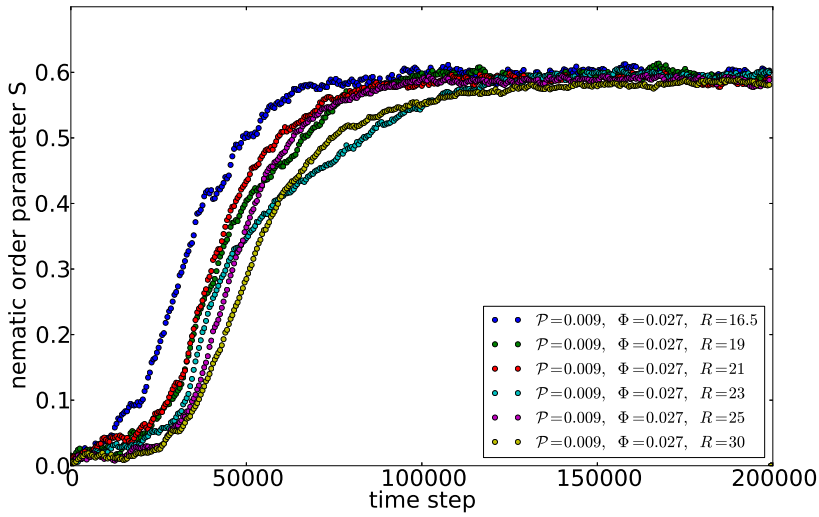

Figure 25: Time evolution of the order parameter for $\mathcal{P} = 0.009$ and $\Phi = 0.027$ for different curvature and particle number.

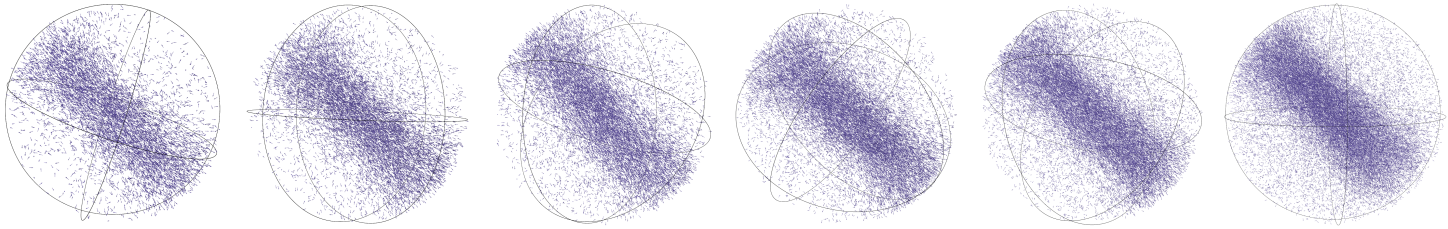

(a) $R = 16.5$ (b) $R = 19$ (c) $R = 21$ (d) $R = 23$ (e) $R = 25$ (f) $R = 30$

Figure 26: Snapshots of the system with $\mathcal{P} = 0.009$ and $\Phi = 0.027$ for increasing radius showing the stream structure.

As stated before, the nematic order parameter does not give a unique description of the system's state. We therefore want to check if similar order parameter values actually correspond to similar configurations of the system and plot configurations with the same Péclet number and filling fraction but with a different curvature and number of particles. We also plot the order parameters of these different systems as a function of time as a reference.

In Fig. 26 one can see the configuration of a system with $\mathcal{P} = 0.009$ and $\Phi = 0.027$ for different radii and particle numbers. All snapshots show the stream configuration and the order parameter is the same for all systems (Fig. 25). We see that for these values of $(\mathcal{P}, \Phi)$ the change of curvature does not affect the formation of the structures.

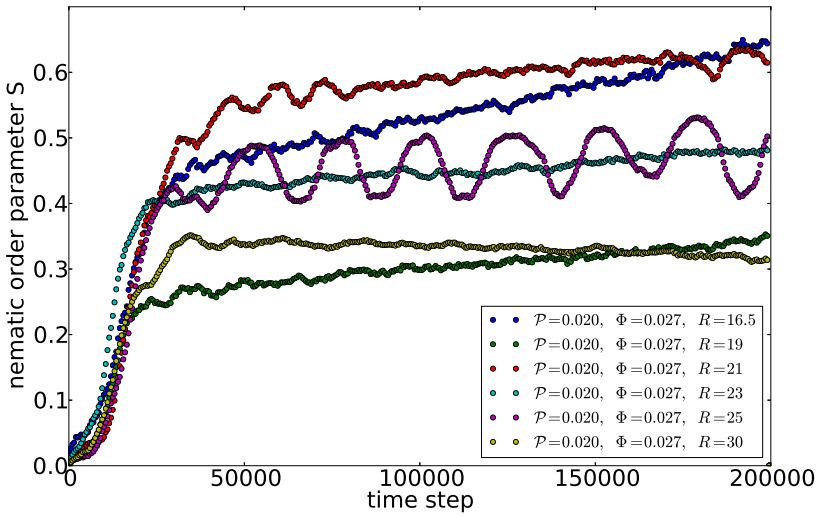

Figure 27: Time evolution of the order parameter for $\mathcal{P} = 0.020$ and $\Phi = 0.027$ for different curvature and particle number.

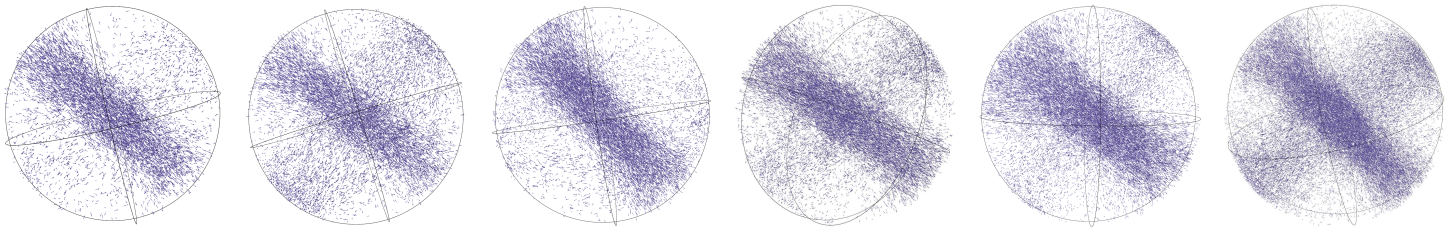

(a) $R = 16.5$ (b) $R = 19$ (c) $R = 21$ (d) $R = 23$ (e) $R = 25$ (f) $R = 30$

Figure 28: Snapshots of the system with $\mathcal{P} = 0.020$ and $\Phi = 0.027$ for increasing radius showing (c) the stream structure and (a),(b),(d),(e) and (f) configurations with stream and belt.

We already saw in Sec. 5.3, Fig. 24, that the influence of the curvature increases with Péclet number and filling fraction. This observation can be confirmed by the order parameter plots and the configuration plots: In Fig. 28 we see snapshots of the system with a higher Péclet number $\mathcal{P} = 0.020$ and the same filling fraction $\Phi = 0.027$ for different radii and particle numbers. Most snapshots show a stream and a belt configuration but the relative intensities of belt and stream vary and for $R = 21$ there is no belt at all. Also the time evolutions of the order parameters,

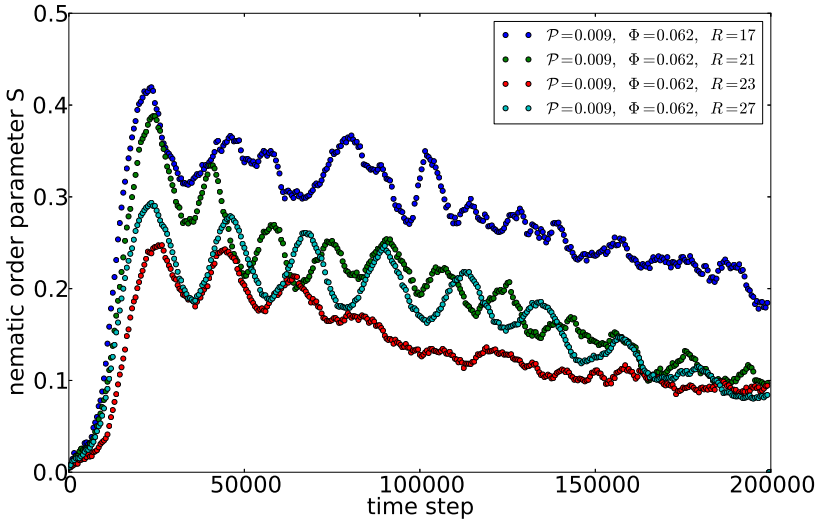

Figure 29: Time evolution of the order parameter for $\mathcal{P} = 0.009$ and $\Phi = 0.062$ for different curvature and particle number.

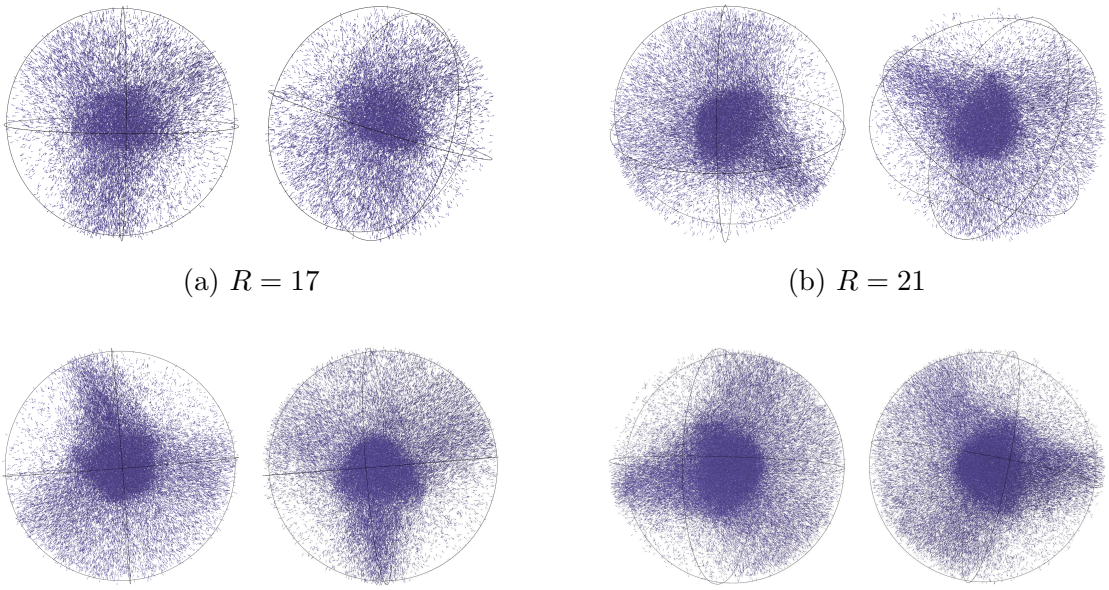

(a) $R = 17$ (b) $R = 21$

(c) $R = 23$ (d) $R = 27$

Figure 30: Snapshots of the system with $\mathcal{P} = 0.009$ and $\Phi = 0.062$ for increasing radius showing the tetrahedral structure. There are two snapshots from different angles (rotated by 90°) for each radius.

shown in Fig. 27, differ more than the ones in Fig. 25. All time evolutions show a similar course but are of different quantitative values.

The same holds for the time evolutions of the order parameters in a system with $\mathcal{P} = 0.009$ and a higher filling fraction $\Phi = 0.062$ in Fig. 29. The snapshots corresponding to these values of $(\mathcal{P}, \Phi)$ show tetrahedral configurations but they

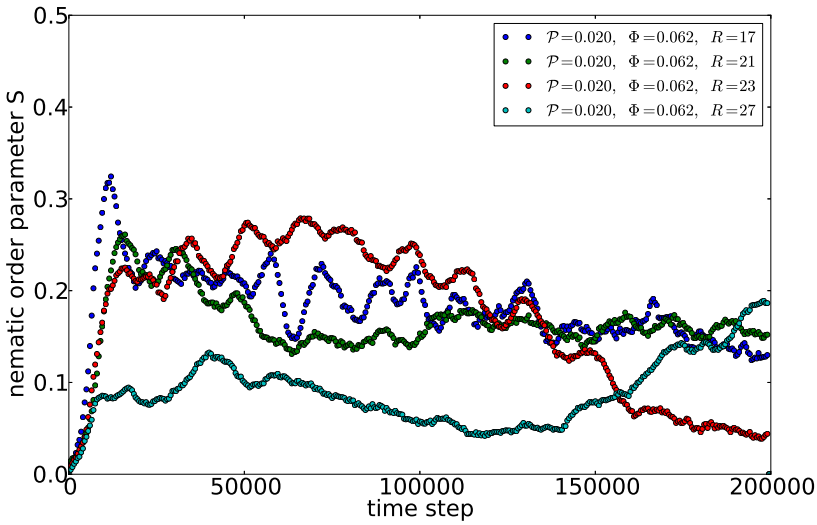

Figure 31: Time evolution of the order parameter for $\mathcal{P} = 0.020$ and $\Phi = 0.062$ for different curvature and particle number.

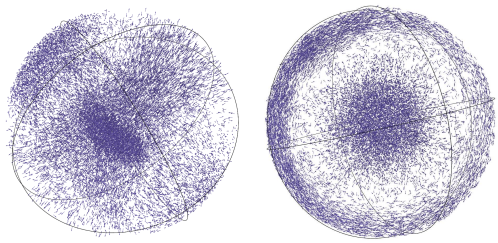

(a) $R = 17$

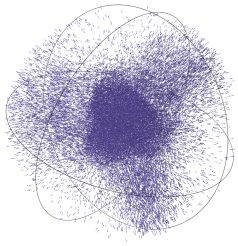

(b) $R = 21$

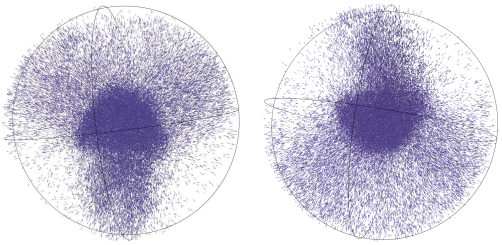

(c) $R = 23$

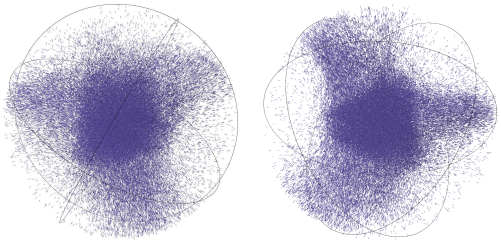

(d) $R = 27$

Figure 32: Snapshots of the system with $\mathcal{P} = 0.020$ and $\Phi = 0.062$ for increasing radius showing (a) a configuration with stream and belt, (b) a Y-like structure and (c) and (d) tetrahedral structures.

look different, especially Fig. 30 (a).

The configurations shown in Fig. 30 with both a high Péclet number $\mathcal{P} = 0.020$ and a high filling fraction $\Phi = 0.062$ vary even more. We find a configuration with stream and belt, a Y-like structure and tetrahedral structures. This is also visible in the order parameter plot in Fig. 31: the time evolutions of the order parameters

look very different.

In Fig. 27, 29 and 31 we see oscillations of the nematic order parameter for certain parameters. To understand this phenomenon we look at videos of the systems. We find out that the oscillations can correspond to a periodic formation and dissolution of clusters (Video 11). In this case the lower order parameter describes the state with a cluster whereas the higher order parameter describes the state without a cluster. Another cause for the oscillation is a change of the relative intensity of structures, for example in Video 12 one can see that the intensities of belt and stream decrease and increase periodically. As the particles moving in the band structure are not aligned with the ones in the stream, the order is lowest when the particles are equally distributed on stream and belt. The oscillations mostly appear for high filling fractions.

Another phenomenon we notice is that in Fig. 27 and 29 the order parameter is still increasing or decreasing after 200 000 time steps for many parameters and has not reached a plateau yet. We run longer simulations with 400 000 time steps for three of these parameter sets. In Fig. 33 one can see the time evolutions of the order parameters we obtained from these simulations. We see that they do not reach a steady state in these longer simulations either: The order parameter increases or decreases further. For two parameter sets the graph starts oscillating in the end which could be the beginning of a steady state.

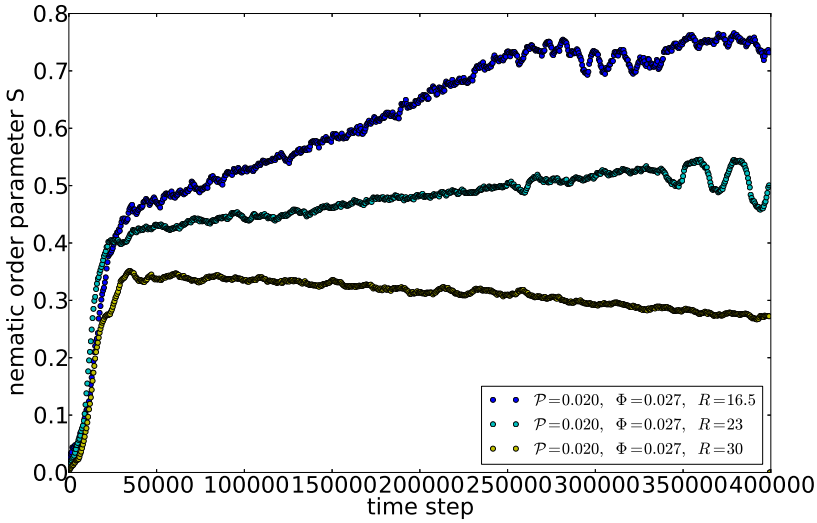

Figure 33: Time evolution of the order parameter for $\mathcal{P} = 0.009$ and $\Phi = 0.027$ over a length of 400 000 time steps for different curvature and particle number.

Looking at the videos of the systems with $R = 16.5$ (see Video 13) and $R = 23$, we find the reason for the increase of S: Both show a configuration with stream

and belt with a decreasing intensity of the belt. For $R = 16.5$ the belt completely vanishes after approximately 210 000 time steps. The oscillations in the end can again be explained by the formation and dissolution of clusters.

5.5 Summary of results

In the previous sections we presented how the collective behaviour of the active swimmers is influenced by the Péclet number $\mathcal{P}$, the filling fraction Φ, the radius R and thus the curvature κ and the total number of particles N by examining the system's nematic order parameter S and investigating snapshots and videos of the configurations. We found a phase transition from an isotropic to a nematic state and back to a less ordered state when varying Péclet number and filling fraction. Except for the isotropic state the system always forms one or a combination of four different structures: a stream, a Y-like, a tetrahedral or a belt structure. We found out that it does not make a significant difference whether we change the filling fraction by varying the radius or the particle number, for most Péclet numbers the results are roughly the same. Curvature and particle number only determine the behaviour for very low noise and thus high Péclet number.

6 Discussion

One of the main sources of error in our results is the assumption that the system has reached the steady state after 150 000 time steps for all parameter values. As we have seen in Sec. 5.2.2 and 5.4, this is not always true. For some parameter sets the transient sets in late (Fig. 20), for other sets there is a slow, continuous change of order parameter over a long time (Fig. 33). Although our assumption is true for most values we investigated, it still reduces the validity of our results, for example the phase diagram. It is important to keep in mind that especially for parameters close to the phase transition line the averaged order parameter should be treated with caution. In spite of this the assumption can be justified because it holds true for most values we investigated.

Another weak point is the order parameter itself. As stated several times before, it only indicates the nematic order of the system but not order in general. It would be useful to calculate an order parameter that takes the topology of the structures into account. This could also help to quantify and automatise the observations of the structures we now made manually by looking at snapshots and videos.

To get an impression of how our results fit into the context of recent research on active swimmers, we compare them to the results by other groups we presented in

Sec. 3.

6.1 Comparison to the phase diagram by Breier *et al.*

First we compare the phase diagram we obtained in Sec. 5.1 to the work by Breier *et al.* [10] (see Sec. 3.1). In Fig. 34 we see that there is a phase transition from an isotropic state for small values of $(\mathcal{P}, \Phi)$ to a nematic state for higher values in both diagrams. The course of the phase transition line is very similar but in our diagram the transition takes place for lower values of $\mathcal{P}$.

In Fig. 34 (b) the nematic order increases monotonically for increasing $\mathcal{P}$. In our phase diagram Fig. 34 (a) it increases first but decreases again for high Péclet numbers. As we pointed out earlier, this decrease of the order parameter does not actually correspond to decreasing order but to configurations with orientations in very different directions, e.g. the configuration showing a stream and a belt. The fact that we do not see this drop of the order parameter in the results concerning the dynamics of particles in a topology free of curvature of Ref. [10] confirms our assumption that these structures are curvature driven.

In the phase diagram of Ref. [10] the order parameter in the nematic state is generally higher than in our system. Many points show an order parameter close to $S = 1$ whereas the highest values occurring in our system are around $S = 0.7$. Also, we did not find any chiral states in our system.

As the two studied systems differ in important features, we did expect quantitative differences in the phase diagrams. The most remarkable result of the comparison of both diagrams is that the topolgy does not affect the fact that the system transitions from an isotropic to a nematic state when varying Péclet number and filling fraction.

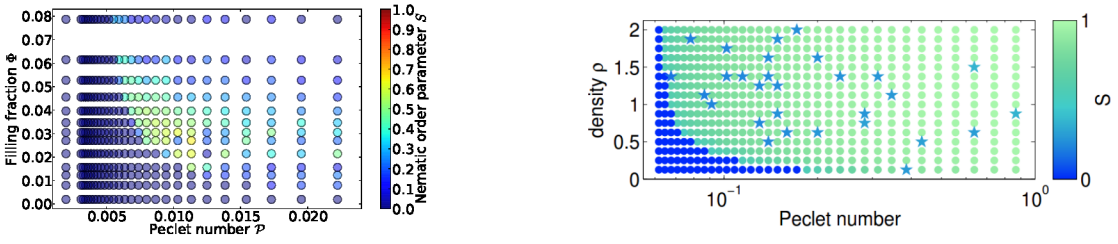

(a) (b)

Figure 34: (a) The phase diagram we plot by varying Péclet number and radius as seen in Sec. 5.1 and (b) the phase diagram by Ref. [10].

6.2 Comparison to the behaviour observed by Vladescu *et al.*

Vladescu *et al.* [12] observed wall hugging in their system of motile bacteria confined within a spherical droplet. We also see a wall hugging phenomenon, the belt structure. In their experiments they also found wall hugging for low filling fractions whereas we only observe the belt configuration for filling fractions $\Phi \geq 0.0125$.

6.3 Comparison to the structures found in experiments by Keber *et al.*

As explained in Sec. 3.3, Keber *et al.* [13] find tetrahedral defect configurations in their experiments on the dynamics of active particles confined to a spherical surface. Studying the configurations by taking snapshots of the system in Sec. 5.2.1, we also observe tetrahedral structures for specific parameter values. They find out that the system oscillates between two symmetric regular tetrahedra, passing through a planar configuration. The tetrahedral structures we observe are often not regular and we do not find an oscillation between different states but configurations that persist for the full length of our simulations.

Keber *et al.* also found a dependency of the structures on the curvature of the spherical surface. For a high radius $R \Leftrightarrow$ low curvature κ they found only configurations with four defects. Decreasing the radius, the system oscillates between a four-defect structure and a configuration where the particles rotate around the equator with two defects at the poles. This is different from what we find, we observe the same kinds of structures for different curvature. Since the system of Keber *et al.* is confined to a spherical surface it is to be expected that curvature plays a stronger role.

6.4 Comparison to the structures found by simulations by Skepnek *et al.*

Skepnek *et al.* [14] find a rotating band of particles similar to our belt structure when simulating active particles confined to a spherical surface (see Sec. 3.4). They observe that the band broadens with increasing noise and eventually disappears. We do not observe a broadening but also find that there are no band structures for high noise. Also they find that the band narrows with the radius R. We do not make equivalent observations (see for example Fig. 28).

7 Conclusion

In this work we investigate the behaviour of active nematic particles confined within a spherical volume by performing molecular dynamics simulations. We find out that the particles' behaviour relates to previous experimental and theoetical results by other groups in similar systems: We observe the phase separation found in a curvature-free system combined with phenomena found on spherical surfaces and in spherical volumes. It is interesting to see that the results in a three-dimensional system with curvature can to a large extent be derived from these single effects.

Another remarkable aspect is that we do not find a significant influence of the degree of curvature. Filling fraction and Péclet number are the parameters decisive for the system's state.

As a next step it could be interesting to investigate more complex topologies and, as mentioned in Sec. 6, find a way to analyse the structures quantitatively. To check if our theoretical results give a good description of active swimmers in a spherical volume it would be helpful to compare them to experimental data.

A Supplemental material

- Video 1: The system with $\mathcal{P} = 0.011$ and $\Phi = 0.021$, showing the time evolution of the stream structure over the full length of the simulation (200 000 time steps).
- Video 2: The system with $\mathcal{P} = 0.008$ and $\Phi = 0.062$, showing the time evolution of the Y-like structure over the full length of the simulation (200 000 time steps).
- Video 3: The system with $\mathcal{P} = 0.010$ and $\Phi = 0.046$, showing the time evolution of the tetrahedral structure over the full length of the simulation (200 000 time steps).
- Video 4: The system with $\mathcal{P} = 0.014$ and $\Phi = 0.016$, showing the time evolution of the belt structure over the full length of the simulation (200 000 time steps).
- Video 5: The system with $\mathcal{P} = 0.013$ and $\Phi = 0.031$, showing the time evolution of the stream and the belt structure combined over the full length of the simulation (200 000 time steps).
- Video 6: The system with $\mathcal{P} = 0.017$ and $\Phi = 0.062$, showing the time evolution of the Y-like structure and the belt structure combined over the full length of the simulation (200 000 time steps).
- Video 7: The system with $\mathcal{P} = 0.017$ and $\Phi = 0.046$, showing the time evolution of the tetrahedral and the belt structure combined over the full length of the simulation (200 000 time steps).
- Video 8: Time evolution of the system with $\mathcal{P} = 0.022$ and $\Phi = 0.031$ over the first 100 000 time steps.
- Video 9: Time evolution of the system with $\mathcal{P} = 0.006$ and $\Phi = 0.031$ over the first 100 000 time steps. The transient is significantly shorter than in Video 8.
- Video 10: The system with $\mathcal{P} =$ and $\Phi =$, showing the occurence of clusters during the transient. *still missing*
- Video 11: The system with $\mathcal{P} = 0.020$ and $\Phi = 0.027$, showing a periodic occurence and dissolution of clusters leading to the oscillation of the nematic order parameter.

- Video 12: The system with $\mathcal{P} = 0.009$ and $\Phi = 0.062$, showing a periodic change of relative intensity of belt and stream structure leading to the oscillation of the nematic order parameter.
- Video 13: The system with $\mathcal{P} = 0.020$, $\Phi = 0.027$ and $R = 16.5$ showing a slow increase of the order parameter caused by a decrease of the intensity of the belt structure over a length of 400 000 time steps.

References

[1] T. Vicsek and A. Zafeiris. Collective motion. *Physics Reports*, 517:71, 2012.

[2] M. Marchetti, J. Joanny, S. Ramaswamy, T. Liverpool, J. Prost, M. Rao, and R. A. Simha. Hydrodynamics of soft active matter. *Reviews of Modern Physics*, 85:1143, 2013.

[3] A. Sokolov, I. S. Aranson, J. O. Kessler, and R. E. Goldstein. Concentration dependence of the collective dynamics of swimming bacteria. *Physical Review Letters*, 98:158102, 2007.

[4] I. L. Bajec and F. H. Heppner. Organized flight in birds. *Animal Behaviour*, 78:777, 2009.

[5] I. R. Fischhoff, S. R. Sundaresan, J. Cordingley, H. M. Larkin, M.-J. Sellier, and D. I. Rubenstein. Social relationships and reproductive state influence leadership roles in movements of plains zebra, equus burchellii. *Animal Behaviour*, 73:825, 2007.

[6] L. Giomi, M. J. Bowick, X. Ma, and M. C. Marchetti. Defect annihilation and proliferation in active nematics. *Physical Review Letters*, 110:228101, 2013.

[7] D. Helbing. Traffic and related self-driven many-particle systems. *Reviews of Modern Physics*, 73:1067, 2001.

[8] John D. Weeks, David Chandler, and Hans C. Andersen. Role of repulsive forces in determining the equilibrium structure of simple liquids. *The Journal of Chemical Physics*, 54:5237, 1971.

[9] Jaroslav M Ilnytskyi and Mark R Wilson. A domain decomposition molecular dynamics program for the simulation of flexible molecules of spherically-symmetrical and nonspherical sites. ii. extension to nvt and npt ensembles. *Computer Physics Communications*, 148:43, 2002.

[10] Rebekka E. Breier, Robin L. B. Selinger, Giovanni Ciccotti, Stephan Herminghaus, and Marco G. Mazza. Spontaneous chiral symmetry breaking in model bacterial suspensions. *arXiv:1406.4423*, 2014.

[11] R. Stocker and J. R. Seymour. Ecology and physics of bacterial chemotaxis in the ocean. *Microbiology and Molecular Biology Reviews*, 76:792, 2012.

[12] I. D. Vladescu, E. J. Marsden, J. Schwarz-Linek, V. A. Martinez, J. Arlt, A. N. Morozov, D. Marenduzzo, M. E. Cates, and W. C. K. Poon. Filling an emulsion drop wit motile bacteria. *Physical Review Letters*, 113, 2014.

[13] Felix C. Keber, Etienne Loiseau, Tim Sanchez, Stephen J. DeCamp, Luca Giomi, Mark J. Bowick, M. Cristina Marchetti, Zvonimir Dogic, and Andreas R. Bausch. Topology and dynamics of active nematic vesicles. *Science*, 345:1135, 2014.

[14] Rastko Sknepnek and Silke Henkes. Active swarms on a sphere. *Physical Review E*, 91:022306, 2015.